Performance and scale-up of adsorptive membrane chromatography

Mark A. Teeters, Thatcher W. Root, Edwin N. Lightfoot*

Department of Chemical Engineering, University of Wisconsin–Madison, 1415 Engineering Drive, Madison, WI 53706, USA

Abstract

Separation efficiency and scalability of Pall Corporation's new Mustang stacked membrane chromatographic devices were investigated, using both the 10-ml and 1-l models and comparing the responses of tracer pulses obtained for conventional and reverse-flow operation. Tracers included AMP, lysozyme, and thyroglobulin, which vary in relative molecular mass from less than 1000 up to 650 000. Both devices showed marked insensitivity to tracer size and flow-rate and gave sharper peaks than would have been expected from conventional 15-μm bead packings. However, reverse-flow peaks were always significantly sharper than those for conventional operation, and the differences were ascribed primarily to non-uniform header residence times. Numerical simulations of the macroscopic flow confirmed that this was indeed the case. This problem was much less pronounced for the 1-l device so scale-up is conservative. © 2002 Elsevier Science B.V. All rights reserved.

Keywords: Membrane chromatography; Adsorption; Computer simulation; Mathematical modelling; Lysozyme; Thyroglobulin; Proteins; Adenosine monophosphate

1. Introduction

The interaction of mass transfer and fluid mechanics is critical in the design of chromatographic systems. The desire to maximize mass transfer rates while minimizing momentum transfer, or pressure drops, has led to chromatographic developments such as perfusive packings [1], cast polymers [2,3], and stacked membranes [4–6], all of which decrease diffusional distances found in resin-based chromatography. Five fundamental ways to increase mass transfer relative to momentum transfer have recently been reviewed [7]. In this study, we characterize the performance of a new stacked-membrane system [8] using both small and large solutes, and determine how well it scales up from a 10-ml to a 1-l bed volume.

Adsorptive membranes [9–11] have been studied for over a decade as an alternative to conventional resin-based chromatography columns. They can exist in a variety of configurations (stacked membranes, hollow fiber membranes, spiral wound membranes) with a variety of adsorptive mechanisms (e.g. ion-exchange, hydrophobic, reversed-phase, affinity). The benefit of adsorptive membranes is the absence of the long diffusion times that often occur in resin-based chromatography. In adsorptive membranes, the interactions between dissolved molecules and the active sites on the membrane occur in convective through-pores rather than in stagnant fluid inside the pores of an adsorbent particle. For this reason, the membrane units have the potential to maintain high efficiencies both at high flow-rates and for use of large biomolecules with small diffusivities.

A second feature of a typical membrane bed is the

*Corresponding author. Tel.: +1-608-262-1092; fax: +1-608-262-5434.

E-mail address: enlightf@facstaff.wisc.edu (E.N. Lightfoot).

large cross sectional area relative to the bed length. These short, wide beds allow high velocities and large volumetric capacity with only modest pressure drops. These features lead to increased throughputs and short residence times, thus reducing protein degradation and denaturation [9]. A large diameter to length ratio, however, introduces the challenge of achieving uniform flow distribution across the membrane. This has been a significant problem in many cases [12,13], reducing the membrane efficiencies to the level of packed beds. Proper design of flow distributors can eliminate this problem, as shown in a recent investigation by Yuan et al. [14,15]. This rational approach to header design suggested distributors that were shown to give uniform flow distribution in numerical simulations and in laboratory prototypes.

Adequate flow distribution is also necessary to maintain the column efficiency when scaling-up a column. Frequently, scale-up is done by optimizing the separation on a small column and increasing the column diameter to meet the desired throughput. If there are no radial variations in the column and flow is evenly distributed across the column cross-section, one should observe identical behavior in a scaled-up separation. However, as the diameter to length ratio increases with column scale-up, it becomes increasingly difficult to maintain uniform flow distribution. Header design and performance become more significant design considerations [16]. In this paper, we investigate the flow distribution of both small and large prototype membrane units and determine how it affects efficiencies and scalability.

2. Theory

2.1. Modeling column efficiency

For differential chromatography, solute effluent concentration is frequently approximated by a Gaussian distribution:

$$c(L, t) = \frac{m_0}{A\varepsilon v} \cdot \frac{1}{\sqrt{2\pi\sigma_t^2}} \cdot \exp\left[\frac{-(t - t_r)^2}{\sigma_t^2}\right] \qquad (1)$$

where c is the concentration of solute exiting a column of length L at time t. Here t_r is the mean

residence time of the solute and σ_t is the standard deviation of its distribution in time. Both microscopic factors, described below in a one-dimensional model, as well as macroscopic factors, such as non-uniform flow through the column, can contribute to the overall dispersion. It may be seen that a single parameter, σ_t^2/t_r^2, is sufficient to characterize the sharpness of the peak. The inverse of this parameter is conventionally defined as the number of theoretical plates, N, and the efficiency of the packing is described by the height equivalent to a theoretical plate, H, where

$$N = \frac{t_r^2}{\sigma_t^2} = \frac{L}{H} \qquad (2)$$

The most reliable means of determining N or H from experimental data is to recognize that these quantities are given by moments of the effluent concentration distribution:

$$t_r = \frac{\int\limits_{-\infty}^{\infty} ct \, \mathrm{d}t}{\int\limits_{-\infty}^{\infty} c \, \mathrm{d}t} \qquad (3)$$

$$\sigma^2 = \frac{\int\limits_{-\infty}^{\infty} c(t - t_r)^2 \, \mathrm{d}t}{\int\limits_{-\infty}^{\infty} c \, \mathrm{d}t} \qquad (4)$$

We must recognize that the number of plates is only defined for a Gaussian distribution and that approximate methods must be used to deal with non-Gaussian distributions. We extend this definition to non-Gaussian distributions [17,18], using moments in our calculations of apparent plate numbers.

2.2. Prediction of plate height

To predict the theoretical plate height of a packed bed in terms of underlying transport and thermodynamic parameters, we will use the model proposed by Athalye et al. as a basic reference [19]. The dispersive mechanisms considered are the mass transfer through a diffusional boundary layer about

the particle, intraparticle diffusion to and from the adsorption sites, the finite kinetics of the adsorption–desorption process, and interparticle axial dispersion resulting from axial diffusion and local flow non-uniformities between particles. The model provides a dimensionless plate height, $h = H/d_p$, which is the height of a theoretical plate divided by the average particle diameter, and has the form [19]:

$$h = \frac{2}{Pe_E} + \frac{(1-u)^2}{3(1-\varepsilon_b)} \cdot (ReSc)$$
$$\cdot \left[\frac{1}{Nu_{BL}} + \frac{m}{Nu_{IP}} + \frac{m'}{Da} \right] \qquad (5)$$

In principle, the magnitudes of all broadening mechanisms can be predicted from separately measured properties. It should be noted that these microscopic sources of dispersion occur on a distance scale δ of the order of particle diameter d_p and that the microscopic dispersion always increases in the direction of flow. We will use this model to compare typical packed bed efficiencies to experimentally measured membrane efficiencies.

2.3. Non-ideal behavior

Not included in the above model are two macroscopic sources of dispersion: macroscopic non-uniform flow in the packing and non-uniform residence time distributions in the inlet and outlet distributors. These tend to occur on a distance scale Δ much greater than the particle diameter d_p. This flow through a chromatographic column is normally characterized by very low Reynolds numbers:

$$Re \equiv \frac{\rho v d_p}{\mu} \ll 1 \qquad (6)$$

where v is the interstitial velocity, ρ is the fluid density, and μ is the fluid viscosity. Such flows are described by the creeping flow equations of continuity and motion [20]:

$$(\nabla v) = 0 \qquad (7)$$

$$\nabla^2 v = \frac{1}{\mu} \cdot \nabla P \qquad (8)$$

These equations are both linear in velocity, and it follows that these flows are reversible as they change

sign but not magnitude with the sign of the driving pressure. Flow through porous headers and columns that follow Darcy's law is an example of such a reversible flow [21]:

$$v_0 = v\varepsilon_b = -\frac{\kappa}{\mu} \cdot \nabla P \qquad (9)$$

Here ε_b is the void fraction and κ is the permeability of the medium. Reversing the pressure gradient reverses the direction but not the magnitude of the velocity; hence, each fluid element will retrace the path originally made in the opposite direction.

Recall that the microscopic dispersion occurring on a length scale δ is irreversible, that is invariant to changes in the direction of flow, and that fluid motions occurring on a length scale Δ are reversible. This provides the basis of what we will next define as the reverse-flow technique: if the direction of flow is reversed when a small pulse of solute is halfway down the column and the solute flows back out the former inlet, any dispersion caused by macroscopic flow variations will be eliminated. The microscopic dispersion, however, irreversible and independent of the direction of flow, will continue and be additive as the solute flows up the column. The resulting elution profile will include only irreversible sources of dispersion. This experiment allows one to decouple the effects of microscopic and macroscopic dispersion, and comparison of a reverse-flow dispersion test to a conventional dispersion test allows us to quantify their relative effects [12,22,23].

2.4. Interaction of column proper and headers

The effect of the header is to increase both solute residence time and dispersion. Modeling the header and column proper in series and following the additivity of moments (see for example Lightfoot et al. [24]) gives

$$\sigma_{tot}^2 = \sigma_{col}^2 + \sigma_{head}^2 \qquad (10)$$

The individual contributions to the total variance are calculated by numerical integration of reverse-flow elution curves, giving σ_{col}^2, and forward-flow elution curves, giving σ_{tot}^2. The effective number of plates can be written as:

$$N_{\text{eff}} = \frac{t_{\text{col}}^2}{\sigma_{\text{col}}^2 + \sigma_{\text{head}}^2} = \frac{t_{\text{col}}^2}{\sigma_{\text{col}}^2} \cdot \left(\frac{1}{1 + \sigma_{\text{head}}^2/\sigma_{\text{col}}^2}\right) \quad (11)$$

Note that the residence time in the header is not included in the numerator because it does not contribute to the separation capability of the unit. It is of practical interest to understand how the above terms change when the solute is retained. The solute retention may be described by a solute retention factor with an operational definition of

$$k' = \frac{t_{\text{col}} - t_0}{t_0} \quad (12)$$

where t_0 is the mean residence time of a small pulse of a nonadsorbed tracer. An increase in k' will cause both an increase in the column retention time, t_{col}, and the column dispersion, σ_{col}^2, while the header dispersion, σ_{head}^2, is nearly independent of k'. The header dispersion will thus have less effect on the observed number of plates, described by Eq. (11), under conditions where the solute is highly retained.

3. Experimental

3.1. Materials

All chemicals and proteins used were from Sigma (St. Louis, MO, USA). Lysozyme and thyroglobulin were dissolved at 10 mg/ml in 10 mM 2-(N-morpholino)ethanesulfonic acid (MES) and 1 M NaCl at pH 5.5. Adenosine monophosphate (AMP) was dissolved at 1 mg/ml in 10 mM MES and 1 M NaCl at pH 5.5. All buffers were prepared with 18 MΩ water from US Filter (Sturbridge, MA, USA). The mobile phase used for all dispersion tests was a 10 mM MES buffer solution, pH 5.5. For non-adsorbing dispersion tests, 1 M NaCl was added, while for adsorbing dispersion tests a lower NaCl concentration was used to achieve desired retention.

3.2. Apparatus

Two stacked-membrane columns were analyzed: a 0.94 cm length×3.7 cm I.D. Pall Mustang-S (Ann Arbor, MI, USA) with a 10-ml nominal bed volume, and a 0.94 cm length×36.8 cm I.D. unit with a 1-l

nominal bed volume. The Mustang-S membranes are polyethersulfone (PES) membranes chemically modified to produce a sulfonic acid surface. The nominal pore size of the PES membranes is 0.8 μm, and the thickness of each membrane layer is 70–90 μm. The membrane layers are housed in a stainless steel ring with porous frits on each side, and 10-ml Mustang modules are rated to 17 bar and 1-l Mustang modules are rated to 8.2 bar. The Mustang module housing was engineered with a design goal of achieving plug flow. The 10-ml Mustang design consisted of a tapered open gap region above a flat porous frit (Fig. 2), while the 1-l Mustang design consisted of a tapered open gap region above a tapered porous frit (Fig. 8).

Pharmacia's AKTA Explorer and UNICORN control software (Peapack, NJ, USA) were used for all 10-ml Mustang-S experiments. Eluent concentration was monitored by the UV detector used at 280 nm for proteins (thyroglobulin and lysozyme) and 260 nm for nucleotides (AMP). For the 1-l Mustang-S experiments, a Pall/Filtron 1000 l Quattro pump (Northborough, MA, USA) was used. All tubing was 1/2 in. I.D. (1 in.=2.54 cm) and an Optek UV concentration monitor Model 316/AF46 (Essen, Germany) was used along with a laboratory-developed Visual Basic program to record the eluent data. In order to have manual control over the direction of flow, two 90° switching valves and two tee connections were set up as seen in Fig. 1.
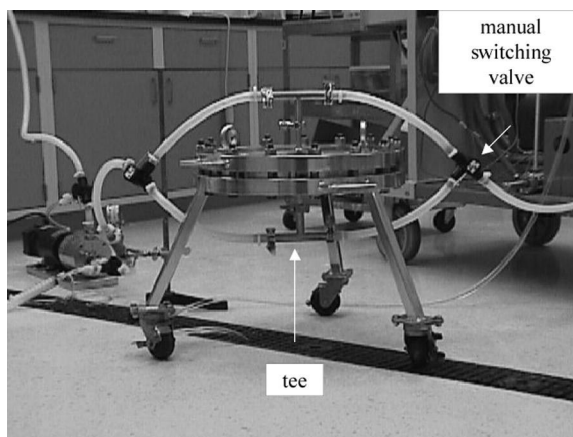

Fig. 1. Photo of 1-l Mustang (I.D.=36.8 cm), switching valves, and tee connections.

3.3. Procedures

The Mustang-S modules were cleaned with five column volumes (CVs) of 1 M NaOH, regenerated with five CVs of 1 M NaCl, and equilibrated with five CVs of the buffer solution prior to dispersion tests. For the 10-ml Mustang-S, 100-µl injections of the above mentioned solutes were made at flow-rates from 10 to 50 ml/min. For the reverse-flow dispersion tests, the direction of flow was reversed at a time equal to one-half the solute residence time of the corresponding forward-flow experiment. Replicates were made of each run at each flow-rate. The peripheral volume and dispersion were measured by the effluent profiles of corresponding injections in the absence of the column. A similar procedure was followed for the 1-l Mustang-S, with the exception of the injection size which was scaled up to be the same percentage of the bed volume. There, 10-ml injections of lysozyme were made at flow-rates of 1.2 and 2.3 l/min.

4. Simulation

The elution curves of a small pulse of solute traveling through the 10-ml and 1-l Mustang-S modules were simulated using the intrinsic membrane dispersion from the reverse-flow experiments and a priori predictions of the macroscopic flow. Conceptually, the column may be depicted as a number of one-dimensional columns in parallel, each representing a single streamline through the actual frit and column. Each will have a time delay representative of the time it takes the solute to pass through the column header, and each column has an intrinsic dispersion equal to that given by the reverse-flow experiments. Here we will describe the physical system and relevant parameters, the simulation of the macroscopic flow, and the prediction of the elution curves.

4.1. System description

The system being simulated is a small pulse of lysozyme traveling through the 10-ml and 1-l Mustang-S modules at one CV/min. The necessary parameters for the simulation of the macroscopic

Table 1
Parameters used in simulating the macroscopic flow through the 10-ml and 1-l Mustang units

	Void fraction	Permeability (cm^2)
Frit	0.3	1.1×10^{-7}
Membrane	0.585	9.2×10^{-10}

flow are the permeabilities and void fractions of the porous frit and stacked membrane, which are found in Table 1, and the viscosity of the mobile phase, which was equal to 1 centipoise. In both units there is an open region containing no frit. This is approximated as a potential flow region with a void fraction equal to one. No-flux boundary conditions exist at the walls and the center of the column, and constant-pressure boundary conditions exist across the top and mid-section of the column. The constant pressure boundary conditions were first estimated using Darcy's law and iteratively changed to get the desired flow-rate.

4.2. Modeling macroscopic flow

The macroscopic flow through the chromatography columns was predicted using MATLAB. Combination of Darcy's law (Eq. (9)) with the continuity equation for an incompressible fluid (Eq. (8)) gives an equation for the pressure field in the column

$$\nabla^2 P = 0 \tag{13}$$

Because of the symmetry of the column, the macroscopic flow is described as a function of the axial position and radius and Eq. (13) can be written as

$$\frac{1}{r} \cdot \frac{\partial}{\partial r} r \left(\frac{\kappa}{\mu \varepsilon_b} \right) \cdot \frac{\partial P}{\partial r} + \frac{\partial}{\partial z} \left(\frac{\kappa}{\mu \varepsilon_b} \right) \cdot \frac{\partial P}{\partial z} = 0 \tag{14}$$

The partial differential equation in Eq. (14) is solved using the finite element method in MATLAB's PDE solver, resulting in the pressure field throughout the column and header. The velocity field in each region is solved using Darcy's law (Eq. (9)). Streamlines through the column and header are determined by numerical integration of the velocity field. A third-order Runge–Kutta method is used by MATLAB,
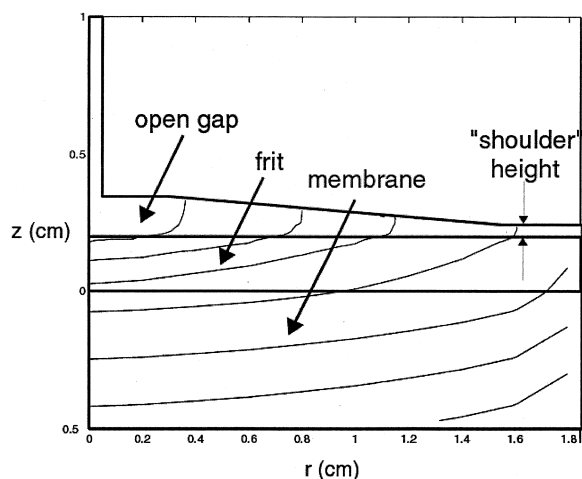
Fig. 2. Simulation of the macroscopic flow through the 10-ml Mustang. Each line represents the position of the center of mass of the solute band at a constant residence time.

starting at points across the middle of the column. The residence times along each streamline are calculated, giving us the time and position of the center of mass of the solute band as it travels down the column [15]. Fig. 2 shows the position of the solute band at different times in the 10-ml Mustang-S.

4.3. Simulating elution profiles

The solute concentration profile along each streamline through the column is broadened by the addition of intrinsic membrane dispersion equal to that determined by reverse-flow experiments. It is assumed that no dispersion occurs along each streamline in the header and that no dispersion occurs across streamlines. Because the actual volume eluted along each streamline varies as a function of the column radius, an appropriately weighted sum of the concentration profiles is made at the column exit. The result is an elution curve that includes dispersion due to both microscopic and macroscopic factors.

5. Results and discussion

5.1. 10-ml Mustang-S dispersion tests

Forward-flow and reverse-flow dispersion tests

were run on the 10-ml Mustang-S using AMP, lysozyme, and thyroglobulin as tracers under conditions where they were not retained by the membrane. The tests were run at flow-rates from 10 to 50 ml/min. Fig. 3 shows forward-flow and reverse-flow elution curves of lysozyme at 10 and 50 ml/min. The reverse-flow elution curves are both sharper and more symmetrical than the corresponding forward-flow curves, indicating significant flow maldistribution. At 10 ml/min, the reverse-flow curve gives about 200 apparent plates, which is impressive for a membrane stack only 0.97 cm thick. The corresponding forward-flow curve, however, shows significant tailing and only gives 30 apparent plates. Because the intrinsic resolution of the short membrane stack is very high, uniform flow distribution across the membrane becomes particularly important.

Fig. 3 also depicts the effect of flow-rate on the intrinsic membrane dispersion. The reverse-flow elution curves at the different flow-rates are very similar, with only slightly more dispersion occurring at the high flow-rate. The intrinsic dispersion occurring in the stacked membrane is minimal and is relatively insensitive to a fivefold increase in flow-rate. This behavior and a summary of all experimental data on the 10-ml Mustang is shown in the Van Deemter plot in Fig. 4, where the theoretical plate heights are plotted against a scaled velocity. For comparison to the performance of a typical chroma-
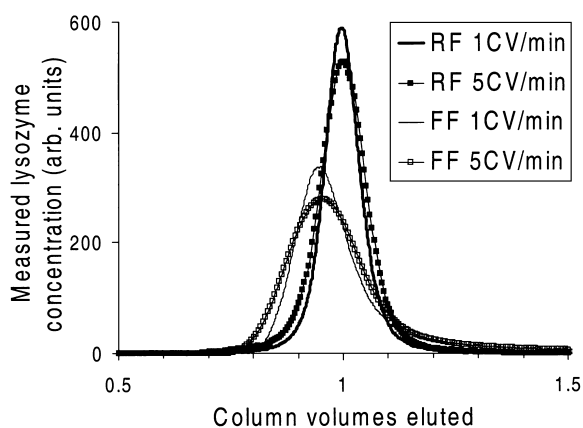

Fig. 3. Comparison of forward-flow and reverse-flow elution profiles from the 10-ml Mustang. Small injections of lysozyme under non-retaining conditions were studied at flow-rates of one and five column volumes per minute.
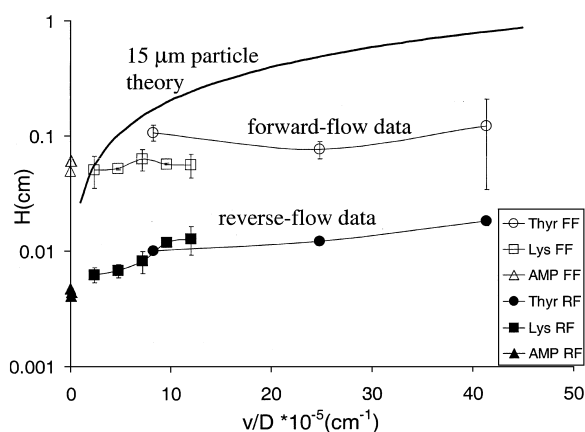
Fig. 4. Plate height vs. scaled velocity for all forward-flow and reverse-flow dispersion tests using the 10-ml Mustang. For comparison, the plate heights for an ideal bed packed with 15-μm particles were predicted using Eq. (5).
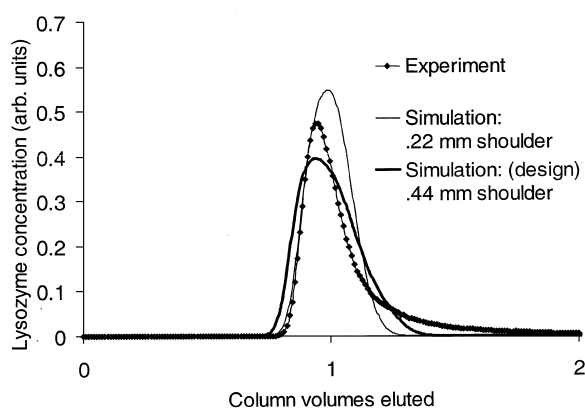

Fig. 5. Comparison of experimental elution curve with curves simulated using a range of expected header configurations. The experimental and simulated profiles are of a non-adsorbing tracer eluting from the 10-ml Mustang.

tography column, the plot also includes the behavior representative of a pulse of lysozyme traveling through a bed packed with 15-μm particles, with H predicted by Eq. (5).

The intrinsic membrane plate heights determined by the reverse-flow experiments are over an order of magnitude lower than the plate heights predicted for 15-μm particles, and only increase slightly with large increases in scaled velocity. There are only modest increases in H when going from the small solutes, AMP ($M_r = 345$) and lysozyme ($M_r \approx$ 14 300), to the large solute, thyroglobulin ($M_r \approx$ 650 000). This is a major strength of membranes and demonstrates promise for separation of even larger molecules including DNA. Because the membrane is not perfectly homogeneous, we believe the small increases in plate heights with velocity are due to diffusion between regions with local velocity variations. The observed increases in plate heights are much smaller than those predicted for the packed bed, which is limited by intraparticle diffusion. The forward-flow plate heights, representative of the actual performance of the 10-ml Mustang-S, are comparable to the packed-bed plate heights at low velocities and are smaller at high velocities. The macroscopic flow is a significant source of dispersion causing the forward-flow plate heights to be an order of magnitude greater than the respective reverse-flow plate heights.

5.2. 10-ml Mustang-S simulations and k' study

The elution curves of a small pulse of lysozyme were simulated as described in Section 4. Fig. 5 shows the results of a MATLAB simulation, where two designs are contrasted with the experimental data. The 0.44-mm shoulder simulation (see Fig. 2 for shoulder height definition) models the design specifications of the housing and captures the tail of the experimental data but under-predicts the peak height. A 0.22-mm shoulder height, on the other hand, provides an upper bound on the peak height but does not capture the tail. The simulation, while not quantitatively precise, captures the essential features of the system and demonstrates the sensitivity of the elution curve to header design.

The dispersion caused by the header was significant when using non-adsorbing tracers, as shown by experiment and simulation, but it has a smaller effect in real separations when the solutes are retained. This is first demonstrated in simulations shown in Fig. 6 for k' values of 1, 3, and 5. As solute retention increases, the simulated elution curves that include header dispersion become more similar to the corresponding elution curves that do not include the header dispersion. The reason for this is that column retention time and column dispersion increase as k' increases, while the header dispersion is nearly independent of k'. As Eq. (11) predicts, the effective number of plates approaches the intrinsic number of
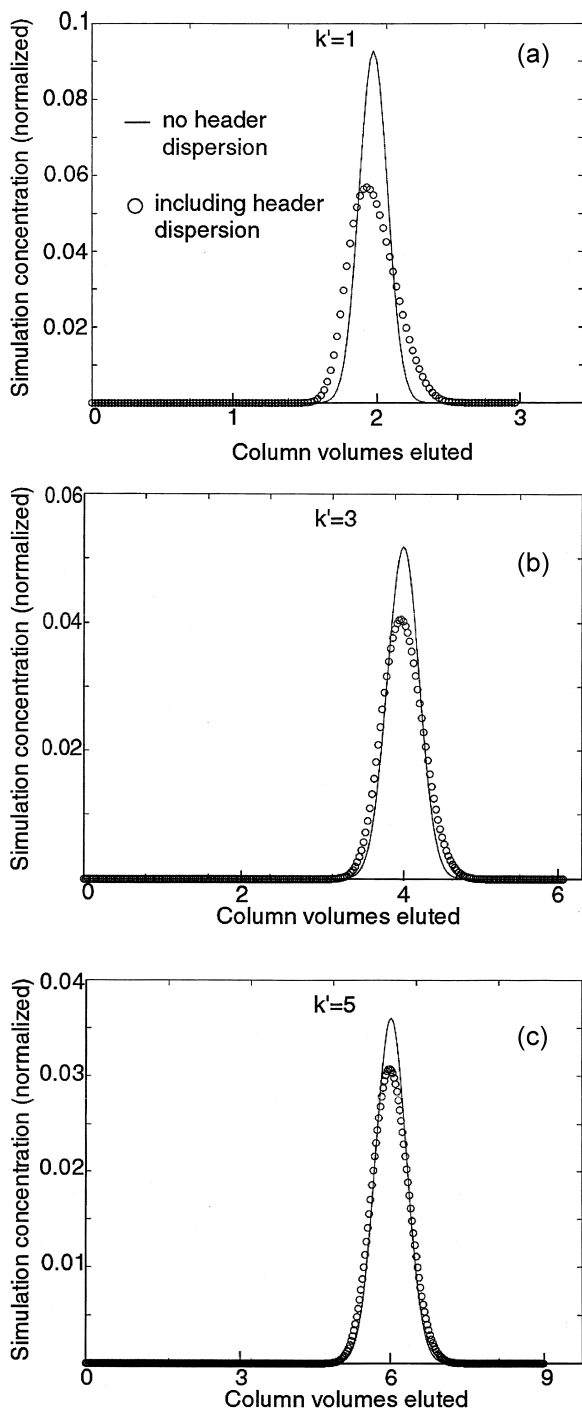
Fig. 6. Simulated concentration profiles for adsorbing tracers eluting from the 10-ml Mustang (circles), with $k' = 1$, 3, and 5 ((a), (b),and (c), respectively). Solid lines represent the elution curves in the absence of header dispersion, determined by reverse-flow experiment.

plates given by the membrane as the dispersion introduced by non-uniform flow becomes a smaller part of the total dispersion. To verify this trend experimentally, we ran dispersion tests with lyso-zyme under varying adsorptive conditions on the 10-ml Mustang-S. The experimentally observed number of plates increased with k', and are shown in Fig. 7 along with the number of plates predicted by simulation and the number of plates observed in the absence of flow maldistribution. The number of plates predicted by simulation was greater than the number observed experimentally. Two factors account for this. Firstly, the simulation did not fully capture the tail observed in experiment (Fig. 4) because of numerical problems simulating the macroscopic flow at the outer edge of the column and the assumption of potential flow in the open gap. The non-uniform laminar flow in this region can lead to significant convective dispersion. Secondly, calculation of apparent plate numbers using statistical moments is extremely sensitive to long tails. This accounts for the discrepancy between the simulation and experimental data, but the general trend is confirmed.

5.3. 1-l Mustang-S simulation and experiment

The 10-ml Mustang-S was scaled up to 1 l at constant bed height (0.94 cm) by increasing the column diameter by a factor of 10. The diameter to length ratio for the 1-l unit is 39, and uniform flow
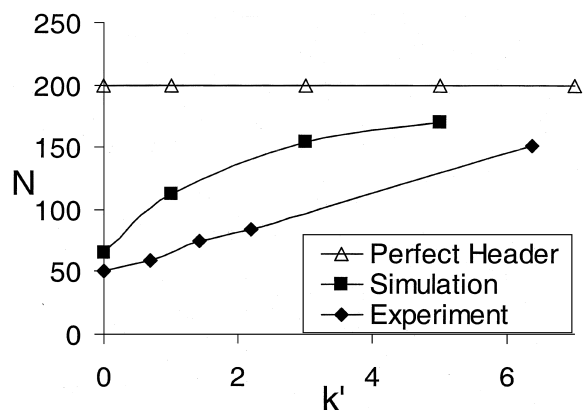

Fig. 7. Number of theoretical plates vs. solute retention for the 10-ml Mustang. Lysozyme was used as the model solute in experiment and simulation.

distribution is essential in maintaining high efficiencies. The distributor design consists of a carefully shaped open gap and porous frit to provide equal residence times for all flow paths through the module. Fig. 8 shows the 1-l design and the simulation of the solute band positions at different times. Our simulation shows that the shaped frit compensates substantially for the different distances each streamline travels by slowing down the fluid towards the center of the column. The result is relatively flat bands with some tailing at the outer edge. The elution curves of a small pulse of lysozyme were predicted using the previously measured intrinsic membrane dispersion to broaden the simulated streamlines through the column. As shown in Fig. 9, the simulated elution curve shows only slightly more dispersion than the 'perfect header' elution curve. The simulation predicts that the designed header on the 1-l Mustang provides better flow distribution than the header on the 10-ml Mustang. This was tested experimentally with forward and reverse-flow lysozyme dispersion tests on the 1-l Mustang-S, shown in Fig. 10. The forward-flow peak is broader and more skewed than the reverse-flow peak, again revealing non-uniform flow distribution. Fig. 11 contrasts the lysozyme dispersion tests on the 10-ml and 1-l units. The 10-ml reverse-flow experiments give lower plate heights than the corresponding 1-l experiments, owing to more irreversible dispersion in

Fig. 9. Simulated concentration profile of a small pulse of lysozyme under non-retaining conditions eluting from the 1-l Mustang (circles). The solid line represents the elution curve in the absence of header dispersion.

the 1-l unit. Compared to the small unit, the respective open gap and porous frit volumes make up a greater percentage of the large unit's volume, and we expect additional irreversible broadening in those regions. While the reverse-flow plate heights are slightly larger for the 1-l module, the forward-flow plate heights are smaller. The header effect is determined by the difference between the reverse-flow and forward-flow plate heights, and the small difference between the two is the consequence of careful header design. The amount of header dispersion, σ^2_{head}, of each unit, observed in experiment and predicted by simulation, is found in Table 2. In each
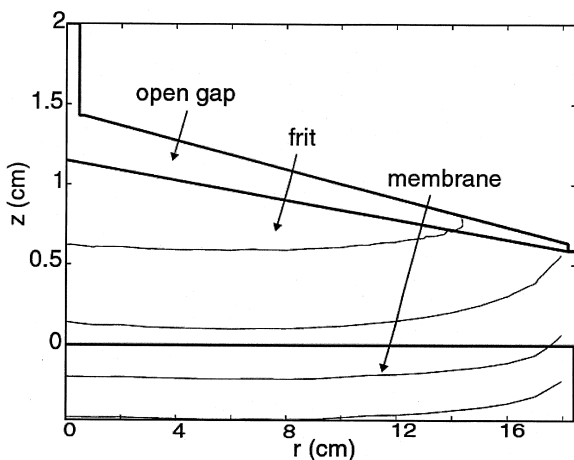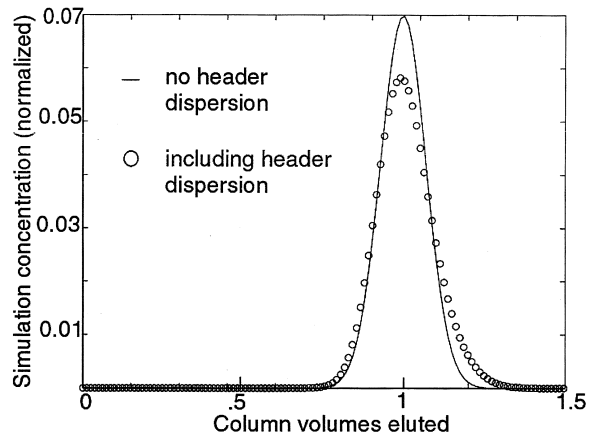

Fig. 8. Simulation of the macroscopic flow through the 1-l Mustang. Each line represents the position of the center of mass of the solute band at a constant residence time.
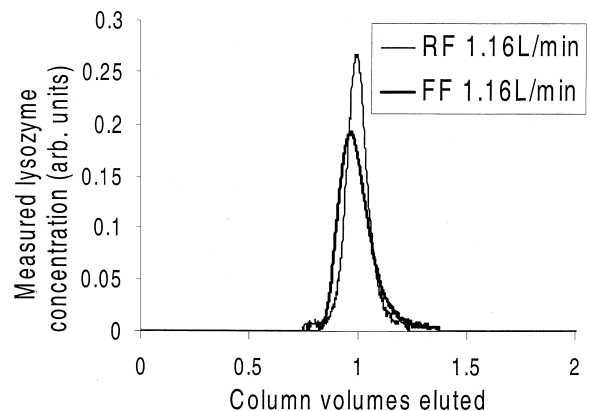

Fig. 10. Comparison of forward-flow and reverse-flow elution profiles from the 1-l Mustang.
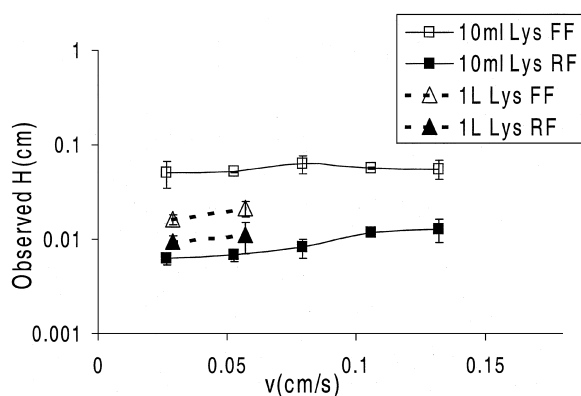
Fig. 11. Forward-flow and reverse-flow plate heights vs. velocity for both the 10-ml and 1-l Mustang units.

case, the simulation again under predicted the header-induced dispersion. However, the smaller amount of header dispersion predicted for the 1-l unit as compared to the 10-ml unit is confirmed by experiment. This is impressive given that the diameter to length ratio of the 1-l unit is 10 times greater that that for the 10-ml unit.

6. Conclusions

In this study, we examined the different factors that contribute to the performance of two prototype stacked-membrane units and the relative importance of each factor at varying operating conditions and column sizes. The intrinsic broadening found in the Mustang-S membranes is minimal and remains small at high velocities and with use of large biomolecules. The intrinsic membrane plate heights are more than one order of magnitude lower than plate heights predicted for a typical chromatography column packed with 15-μm particles. The non-uniform flow distribution does significantly reduce the observed efficiency of the 10-ml unit when using non-adsorbing tracers. However, for adsorbing species, the flow

distribution becomes less significant and the observed efficiency approaches the intrinsic membrane efficiency. The 1-l unit was found to have adequate flow distribution and maintained plate heights less than those predicted for the 15-μm particle bed, despite the high diameter-to-length ratio.

7. Nomenclature

A	column cross sectional area (cm^2)
c	effluent solute concentration (mg/ml)
Da	Damkohler number, defined as $d_p^2 k_a / 4 D_A$
D_A	effective solute diffusivity in pore liquid (cm^2/s)
D_F	effective solute diffusivity in the percolating solution (cm^2/s)
d_p	diameter of a stationary-phase particle (μm)
E	convective axial dispersion coefficient (cm^2/s)
ε	column void fraction
ε_b	interstitial (interparticle) void fraction in a packed bed
ε_p	intraparticle inclusion porosity of a solute
H	height equivalent to a theoretical plate (HETP) or plate height (cm)
h	reduced plate height, defined as H/d_p
k'	capacity or solute retention factor
k_a	forward adsorption rate constant
k_c	concentration-based fluid mass-transfer coefficient (cm/s)
K_D	ratio of solute concentrations in the adsorbent pores and in the external solution at equilibrium
k_p	lumped parameter mass-transfer coefficient inside the particle pore (cm/s)
κ	permeability constant of porous materials (cm^2)
L	column length (cm)
m	parameter in the reduced plate height expression, defined as $D_F/D_A \times 1/\varepsilon_p K_D$
m'	parameter in the reduced plate height expression, defined as $3/2 \cdot m \cdot (K_D/1 + K_D)$
m_0	mass of solute fed to the column in a pulse (mg)
μ	fluid viscosity (g/cm s)
N	number of theoretical plates

Table 2
Observed and simulated header dispersion occurring in the 10-ml and 1-l Mustang units

	$\sigma_{head,obs}$ (s)	$\sigma_{head,sim}$ (s)
10 ml	10.9	6.0
1 l	8.9	4.9

Nu_{BL} fluid-phase Nusselt number, defined as $k_c d_p / D_F$

Nu_{IP} intraparticle Nusselt number, defined as $k_p d_p / D_A$

P pressure (Pa)

Pe_{E} particle-based dispersion Peclet number, defined as $d_p V / E$

Re Reynolds number, defined as $d_p V \rho / \mu$

ReSc reduced velocity or diffusion Peclet number, defined as $d_p V / D_F$

ρ fluid density (g/cm^3)

σ_{col} standard deviation of the solute distribution in the column alone (s)

σ_{head} standard deviation of the solute distribution in the column header alone (s)

σ_t standard deviation of solute distribution in time (s)

t time (s)

t_0 mean residence time of a nonadsorbed tracer (s)

t_{col} mean residence time of a solute in the column alone (s)

t_r mean residence time of a solute (s)

u fraction of solute in the moving fluid phase at long times

v interstitial solute velocity (cm/s)

V magnitude of the interstitial percolating velocity (cm/s)

v_0 superficial fluid velocity (cm/s)

References

[1] N.B. Afeyan, N.F. Gordon, I. Mazsaroff, L. Varady, S.P. Fulton, Y.B. Yang, F.E. Regnier, J. Chromatogr. 519 (1990) 1.

[2] M. Petro, F. Svec, J.M.J. Frechet, J. Chromatogr. A 752 (1996) 59.

[3] S. Hjerten, Y.M. Li, J.L. Liao, J. Mohammad, K. Nakazato, G. Pettersson, Nature 356 (1992) 810.

[4] K.G. Briefs, M.R. Kula, Chem. Eng. Sci. 47 (1992) 141.

[5] J.A. Gerstner, R. Hamilton, S.M. Cramer, J. Chromatogr. 596 (1992) 173.

[6] T.B. Tennikova, F. Svec, J. Chromatogr. 646 (1993) 279.

[7] E.N. Lightfoot, J.S. Moscariello, M.A. Teeters, T.W. Root, in: A. Velayudhan, A.S. Rathore (Eds.), Scale-Up and Optimization in Preparative Chromatography, Marcel Dekker, New York, in press.

[8] Mustang Modules for Chromatography of Biomolecules, Pall BioPharmaceuticals, Ann Arbor, MI, 2000.

[9] D.K. Roper, E.N. Lightfoot, J. Chromatogr. A 702 (1995) 3.

[10] C. Charcosset, J. Chem. Technol. Biotechnol. 71 (1998) 95.

[11] J. Thommes, M.R. Kula, Biotechnol. Prog. 11 (1995) 357.

[12] D.K. Roper, E.N. Lightfoot, J. Chromatogr. A 702 (1995) 69.

[13] D. Josic, J. Reusch, K. Loster, O. Baum, W. Reutter, J. Chromatogr. 590 (1992) 59.

[14] Q.S. Yuan, A. Rosenfeld, T.W. Root, D.J. Klingenberg, E.N. Lightfoot, J. Chromatogr. A 831 (1999) 149.

[15] Q.S. Yuan, Ph.D. Thesis, University of Wisconsin–Madison, Madison, WI, 1999.

[16] E.N. Lightfoot, Am. Lab. 31 (1999) 13.

[17] M.S. Jeansonne, J.P. Foley, J. Chromatogr. 594 (1992) 1.

[18] P. Schneider, J.M. Smith, AIChE J. 14 (1968) 762.

[19] A.M. Athalye, S.J. Gibbs, E.N. Lightfoot, J. Chromatogr. 589 (1992) 71.

[20] R.B. Bird, W.E. Stewart, E.N. Lightfoot, Transport Phenomena, Wiley, New York, 1960.

[21] T. Farkas, G.M. Zhong, G. Guiochon, J. Chromatogr. A 849 (1999) 35.

[22] M. Kaminski, J. Chromatogr. 589 (1992) 61.

[23] J. Moscariello, G. Purdom, J. Coffman, T.W. Root, E.N. Lightfoot, J. Chromatogr. A 908 (2001) 131.

[24] E.N. Lightfoot, J.L. Coffman, F. Lode, Q.S. Yuan, T.W. Perkins, T.W. Root, J. Chromatogr. A 760 (1997) 139.